Fractal Aggregates of Conjugated Polymer in Solution State

Yen-Cheng Li,[†] Kuei-Bai Chen,[†] Hsin-Lung Chen,*[,‡] Chain-Shu Hsu,[†] Cheng-Si Tsao,[§] Jean-Hong Chen,[||] and Show-An Chen[‡]

Department of Applied Chemistry, National Chiao Tung University, Hsin-Chu 30050, Taiwan, Department of Chemical Engineering, National Tsing Hua University, Hsin-Chu 30013, Taiwan, Institute of Nuclear Energy Research, Lungtun, Taoyuan, Taiwan, and Department of Polymer Materials, Kun Shan University, Yung-Kang City, Tainan Hsien 71003, Taiwan

Received May 8, 2006. In Final Form: July 14, 2006

Semirigid conjugated polymers have received much scientific and technological interest due to their unique electrical and photonic semiconducting properties. Spectroscopic studies have indicated that these polymers underwent interchain aggregation in the solution state even at large dilution; however, the origin of this event and the structure of the resultant aggregates remained the crucial issues to be resolved. In the present study, we revealed that the interchain aggregation of a conjugated polymer, poly(2,3-diphenyl-5-hexyl-1,4-phenylenevinylene) (DP6−PPV), in solutions with chloroform and toluene generated network aggregates with the hydrodynamic radii of several micrometers. Small angle neutron scattering (SANS) demonstrated that the internal structure of these aggregates could be characterized by the mass fractal dimensions of 2.2−2.7. The networks were looser in chloroform but became highly compact in the poorer toluene solvent due to severe segmental association. Increasing the temperature alleviated the segmental association in toluene while largely retaining the mass fractal dimension of the aggregates. However, the interchain aggregation was never completely dissipated by the heating, suggesting the existence of two types of segmental association with distinct stability. The highly stable segmental association that could neither be solvated by chloroform nor be disrupted thermally in toluene was attributed to the $\pi-\pi$ complex already present in the DP6−PPV powder used for the solution preparation. The chains tied firmly by this complex formed network aggregates in the solution and hence reduced the entropy of mixing of the polymer. In the poorer toluene solvent, further segmental association took place within the preexisting aggregates, making the networks more compact. This type of segmental association could be disrupted by moderate heating, and its occurrence was ascribed to the poor affinity of the aliphatic side chains of DP6−PPV for toluene.

Introduction

Conjugated polymers have gained much interest due to their unique electrical and photonic semiconducting properties for optoelectronic applications such as polymer light-emitting diodes (PLED).[1−3] This class of polymer is usually composed of a semirigid conjugated backbone attached with flexible short side chains to render the polymer nominally soluble in common organic solvents and hence facilitate the device processing using spin or drop casting techniques. Spectroscopic studies have indicated that conjugated polymers undergo interchain aggregation in the solution state even at large dilution.[4−7] However, the origin of this event and the structure of the resultant aggregates still remain the crucial issues to be resolved as the presence of aggregates even in trace amount can have profound impact on the photophysics of these materials.[4,8−11] Considering that the aggregation is not accompanied with apparent macrophase separation and it may take place at very low polymer concentration, it becomes difficult to make a straightforward connection of this process to the phase transformations having been encountered in solutions of rigid macromolecules, such as crystallization and lyotropic nematic phase formation.[12] Micellization driven by the possible amphiphicility of the polymer due to the disparity in the solvent affinity of the conjugated backbone and the aliphatic side chains may be a plausible mechanism for the aggregation.[13] Nevertheless, more in-depth studies are necessary to test this postulate, in particular as to whether the micelles are "segmental micelles" (formed by the local association of segments) or "molecular micelles" (formed by the aggregation of the whole polymer molecules as encountered in block copolymer solutions).

In this paper, we investigate the interchain aggregation behavior of a conjugated polymer dissolved in two solvents of different qualities. Here we use small angle neutron scattering (SANS) as the major tool for resolving the aggregation behavior. SANS is known as a powerful tool for characterizing the conformational structure and aggregation behavior of macromolecules in

* Corresponding author. Phone: +886-3-5721714. Fax: +886-3-5715408. E-mail: hslchen@mx.nthu.edu.tw.

[†] National Chiao Tung University.

[‡] National Tsing Hua University.

[§] Institute of Nuclear Energy Research.

[||] Kun Shan University.

(1) Burroughes, J. H.; Bradly, D. D. C.; Brown, A. R.; Marks, R. N.; Mackay, K. Friend, R. H.; Burns, P. L.; Holmes, A. B. *Nature (London)* **1990**, *347*, 539.

(2) Friend, R. H.; Gymer, R. W.; Holmes, A. B.; Burroughes, J. H.; Marks, R. N.; Taliani, C.; Bradley, D. D. C.; dos Santos, D. A.; Brédas, J. L.; Löglund, M.; Salaneck, W. R. *Nature (London)* **1999**, *397*, 121.

(3) Spreitzer, H.; Becker, H.; Kluge, E.; Kreuder, W.; Schenk, H.; Demandt, R.; Schoo, H. *Adv. Mater.* **1998**, *10*, 1340.

(4) Nguyen, T. Q.; Doan, V.; Schwartz, B. J. *J. Chem. Phys.* **1999**, *110*, 4068.

(5) Grell, M.; Bradley, D. D. C.; Ungar, G.; Hill, J.; Whitehead, K. S. *Macromolecules* **1999**, *32*, 5810.

(6) Collison, C. J.; Rotherberg, L. J.; Treemaneekarn, V.; Li, Y. *Macromolecules* **2001**, *34*, 2346.

(7) Hsu, J. H.; Fann, W. S.; Tsao, P. H.; Chuang, K. R.; Chen, S. A. *J. Phys. Chem. A* **1999**, *103*, 2375.

(8) Blatchford, J. W.; Jessen, S. W.; Lin, L. B.; Gustafson, T. L.; Fu, D. K.; Wang, H. L.; Swager, T. M.; MacDiarmid, A. G.; Epstein, A. J. *Phys. Rev. B* **1996**, *54*, 9180.

(9) Shi, Y.; Liu, J.; Yang, Y. *J. Appl. Phys.* **2000**, *87*, 4254.

(10) Peng, K. Y.; Chen, S. A.; Fann, W. S. *J. Am. Chem. Soc.* **2001**, *123*, 11388.

(11) Chen, S. H.; Su, A. C.; Huang, Y. F.; Su, C. H.; Peng, G. Y.; Chen, S. A. *Macromolecules* **2002**, *35*, 4229.

(12) Jones, R. A. L. *Soft Condensed Matter*; Oxford: New York, 2002.

(13) Ou-Yang, W. C.; Chang, C. S.; Chen, H. L.; Tsao, C. S.; Peng, K. Y.; Chen. S. A.; Han, C. C. *Phys. Rev. E* **2005**, *72*, 031802.

10.1021/la0612769 CCC: $33.50
Published on Web 11/18/2006

solutions.[14,15] This technique makes use of the distinct contrast in neutron scattering length between deuterated solvent and hydrogenous polymer (or vice versa), which offers decent scattering intensity and effectively reduces the incoherent background for probing the solution structure at relatively low polymer concentration. SANS can effectively complement the spectroscopic techniques such as photoluminescence spectroscopy, where the attribution of the lower energy emission to the presence of aggregates is sometimes complicated by other emission species such as excimers[4,16−19] and chemical defects.[20−23]

In a recent study, Perahia et al. have utilized SANS to probe the aggregate structure of a conjugated polymer, poly(2,5-dinonylparaphenylene ethynylene) (PPE), in the solution with toluene.[24,25] The triple bonds along the backbone imparted conformational rigidity to the molecule; therefore, PPE chains were essentially rodlike. The rodlike molecules were found to aggregate into large flat clusters driven by the $\pi-\pi$ interaction below ca. 40 °C. When the aggregates were too large to freely move in the solution, a transition into a constrained or jammed phase took place, transforming the viscous solution into gel.

The conjugated polymer studied here is poly(2,3-diphenyl-5-hexyl-1,4-phenylenevinylene) (DP6−PPV) with the chemical structure shown below DP6−PPV is an attractive green-emitting

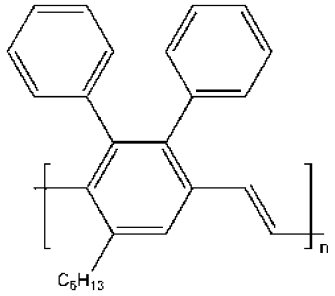

material for PLED application due to its high glass transition temperature, high fluorescence efficiency, and ease of monomer and polymer syntheses.[26−29] In contrast to PPE, the conjugated double bonds in the backbone of DP6−PPV render the chain a certain degree of flexibility, such that its conformation is more properly described by the semirigid "wormlike chain" instead of a rigid rod.[13,30] The entropic gain from the conformational flexibility may enhance the solubility of the polymer in the solution and thus reduces the aggregation power of DP6−PPV compared with that of PPE. Consequently, the structure of the aggregates may be largely different from the compact plate structure formed by PPE. In the present study, we investigated the aggregation behavior of DP6−PPV in chloroform and toluene. Chloroform was considered as a relatively good solvent for the polymer, whereas toluene was a relatively poor one. With the aid of dynamic light scattering (DLS), we will demonstrate that DP6−PPV underwent interchain aggregation in both solvents, generating aggregates with the hydrodynamic radii of several micrometers. The corresponding SANS profiles reveal the network internal structure for these aggregates with the mass fractal dimension of 2.2−2.7. The origin of the interchain aggregation will also be discussed in connection with the highly persistent $\pi-\pi$ complex present in the DP6−PPV powder before dissolution.

Experimental Section

DP6−PPV was synthesized according to the procedure described elsewhere.[26−29] The weight-average molecular weight (M_w) and polydispersity index of the polymer were 448 000 and 1.3, respectively. The polymer solutions with concentrations of 0.1, 0.5, and 1.0 wt % were prepared by dissolving the appropriate amount of the polymer in chloroform and toluene. Deuterated solvents were used for enhancing the contrast in neutron scattering length densities (SLD). The mixtures of polymer and solvent were stirred at ca. 40 °C for 12 h, where macroscopically homogeneous solutions were observed by naked eyes after the stirring. The solutions were allowed to equilibrate at room temperature (ca. 25 °C) for 12 h prior to the SANS and DLS measurements.

The SANS measurements were performed on the 8 m SANS instrument (NG1) at the National Institute of Standard and Technology (NIST).[31] The incident neutron wavelength was $\lambda = 8$ Å with a wavelength dispersion of $\Delta\lambda/\lambda = 0.14$. The configuration of the SANS instrument, including the collimated pinhole size and the sample-to-detector distance, was optimized to give an effectively measured q-range of 0.008−0.12 Å^{-1}. The scattering intensity $I(q)$ was corrected for transmission, background, and parasitic scattering and normalized to an absolute intensity (scattering cross section per unit sample volume) as a function of the scattering vector q, where $q = (4\pi/\lambda)\sin(\theta/2)$ (θ is the scattering length angle).[32] The incoherent backgrounds from the pure solvents were also measured, corrected by the volume fraction displaced by the dissolved DP6−PPV and subtracted from the reduced SANS data. Temperature (calibrated and controlled within ±0.1 °C) of the solution during SANS measurement was achieved by use of a 10-piston heating/cooling block connected to a circulating bath (50/50 mixture of water and ethylene glycol). For the measurement at each temperature, the sample was first held at the prescribed temperature for 30 min followed by data acquisition for another 30 min. This acquisition time was sufficient to give reasonable counting statistics of the scattered intensity (~10^6 counts).

DLS experiments were performed using a Malvern CGS-3 equipment with an ALV/LSE-5003 Multiple-τ digital correlator. A 22-mW laser beam (632.8 nm in wavelength) was passed through a quartz cell holding the solutions, and the scattering intensity was detected at 90° with respect to the incident beam. The scattered light was analyzed with an autocorrelator to generate the normalized electric field-time correlation function, $g^{(1)}(\tau)$.[33,34] For a system exhibiting a distribution of collective motions, $g^{(1)}(\tau)$ can be represented by the superposition of exponential decay functions.

(14) Roe, R. J. *Methods of X-ray and Neutron Scattering in Polymer Science*; Oxford: New York, 2000.
(15) Higgins, J. S.; Benoit, H. C. *Polymers and Neutron Scattering*; Oxford: New York, 1994.
(16) Samuel, I. D. W.; Rumbles, G.; Collison, C. J. *Phys. Rev. B* **1995**, R11573.
(17) Nguyen, T. Q.; Matrini, I. B.; Liu, J.; Schwartz, B. J. *Phys. Chem. B* **2000**, *104*, 237.
(18) Grell, M.; Bradley, D. D. C.; Long, X.; Inbasekaran, M.; Woo, E. P.; Soliman, M. *Acta. Polym.* **1998**, *49*, 439.
(19) Grell, M.; Bradley, D. D. C.; Ungar, G.; Hill, J.; Whitehead, K. S.; *Macromolecules* **1999**, *32*, 5810.
(20) Gong, X.; Iyer, P. K.; Moses, D.; Bazan, G. C.; Heeger, A. J.; Xiao, S. S.; *Adv. Funct. Mater.* **2003**, *13*, 325.
(21) Romaner, L.; Pogantsch, A.; de Freitas, P. S.; Scherf, U.; Gaal, M.; Zojer, E.; List, E. J. W. *Adv. Funct. Mater*. **2003**, *13*, 597.
(22) Gaal, M.; List, E. J. W.; Scherf, U. *Macromolecules* **2003**, *36*, 4236−4237.
(23) Kulkarni, A. P.; Kong, X.; Jenekhe, S. A. *J. Phys. Chem. B* **2004**, *108*, 8689.
(24) Perahia, D.; Traiphol, R., Bunz, U. H. F. *J. Chem. Phys*. **2002**, *117*, 1827.
(25) Perahia, D.; Jiao, X., Traiphol, R. *J. Polym. Sci.*: *Part*: *B* **2004**, *42*, 3165.
(26) Hsieh, B. R.; Antoniadis, H. *Adv. Mater*. **1995**, *7*, 36
(27) Hsieh, B. R.; Yu, Y.; Forsythe, E. W.; Schaff, G. M.; Feld, W. A. *J. Am. Chem. Soc.* **1998**, *120*, 231.
(28) Wan, W. C.; Antoniadis, H.; Choong, V. E.; Razafitrimo, H.; Gao, Y.; Feld, W. A.; Hsieh. B. R. *Macromolecules* **1997**, *30*, 6567.
(29) Hsieh, B. R.; Yu, Y. U.S. Patent 5,945,502, 1999.
(30) Gettinger, C. L.; Heeger, A. J.; Drake, J. M.; Pine, D. J. *J. Chem. Phys.* **1994**, *101*, 1673.
(31) Glinka, C. J.; Barker, J. G.; Hammouda, B.; Krueger, S.; Moyer, J. J.; Orts, W. J. *J. Appl. Crystallogr*. **1998**, *31*, 430.
(32) Cold Neutron Research Facility at the National Institute of Standard and Technology. *NG3 and NG7 30-Meter SANS Instruments Date Acquisition Manual;* 1999.
(33) Schmitz, K. S. *An Introduction to Dynamic Light Scattering by Macromolecules*; Academic Press: Boston, 1990.
(34) Brown. W. *Dynamic Light Scattering*; Clarendon Press: Oxford, 1993.

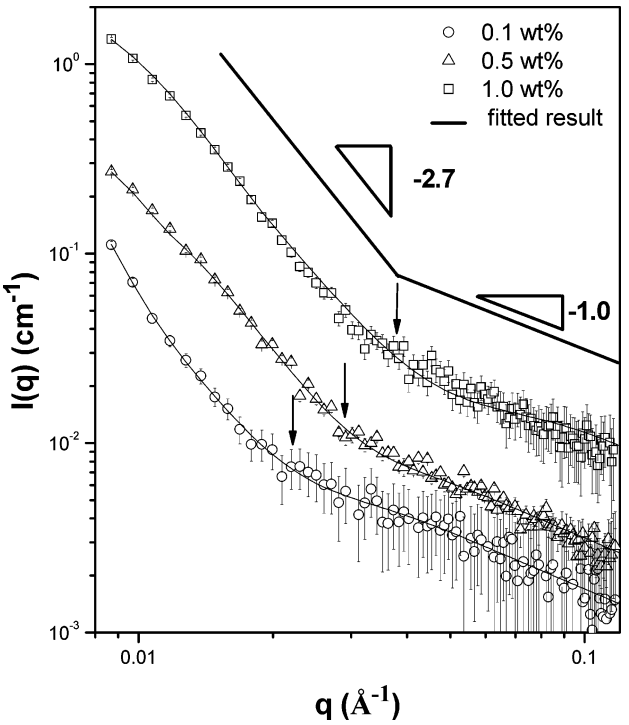

Figure 1. The room-temperature SANS profiles in log−log plots of DP6−PPV in solutions with chloroform at different concentrations. Two power-law regimes were identified in the scattering profiles, irrespective of the concentration. The intensity exhibited a power law of $I(q) \sim q^{-2.7}$ in the middle- to low-region characterizing the mass fractal dimension of the network aggregates. The q-dependence transformed to another power law of $I(q) \sim q^{-1}$ at high q, corresponding to the form factor of the rodlike subchains between the junction points in the networks. The solid curves are the fitted results using the unified equation.

Laplace inversion routine of $g^{(1)}(\tau)$ was performed to yield the distribution of relaxation times $A(\tau)$, viz.

$$g^{(1)}(\tau) = \int_0^\infty A(\tau) \exp(-t/\tau)\, d\tau \quad (1)$$

The translational diffusion coefficient distribution was obtained from $A(\tau)$ and the hydrodynamic radius distribution was eventually obtained using the Stokes−Einstein equation, $R_h = k_B T/(6\pi\eta D)$, where k_B is the Boltzman constant, T is absolute temperature, D is the diffusion coefficient, and η is solvent viscosity.

Result and Discussion

Aggregate Structure in DP6−PPV/Chloroform Solutions. Figure 1 shows the room-temperature SANS profiles of DP6−PPV in the solutions with chloroform at different concentrations. The SANS intensities followed $I(q) \sim q^{-1}$ dependence in the high-q region ($q > \sim 0.03$ Å^{-1}) irrespective of the polymer concentration, indicating the presence of rod entity under large spatial resolution.[14,15] The scattering intensity in this q region was dominated by the form factor of the rod entity, viz.,[15]

$$I(q) = N\Delta\rho^2 V_{rod}{}^2 P_{rod}(q) \quad (2)$$

where $I(q)$ is the absolute intensity in cm^{-1}, N is the number density of rod particles, $\Delta\rho$ is the SLD contrast between the solvent and the particle, V_{rod} is the volume of the rod, and $P_{rod}(q)$ is the form factor function of the rod particle. Let $V_{rod} = z\upsilon_u$, with z and υ_u being the number of monomer units in a rod and volume of a monomer unit, respectively, and $N = cN_{av}/(zM_u)$, with c, M_u, and N_{av} being the concentration in g/mL, molar mass of the monomer unit, and Avogardro's number, respectively, then eq 2 can be reorganized to give

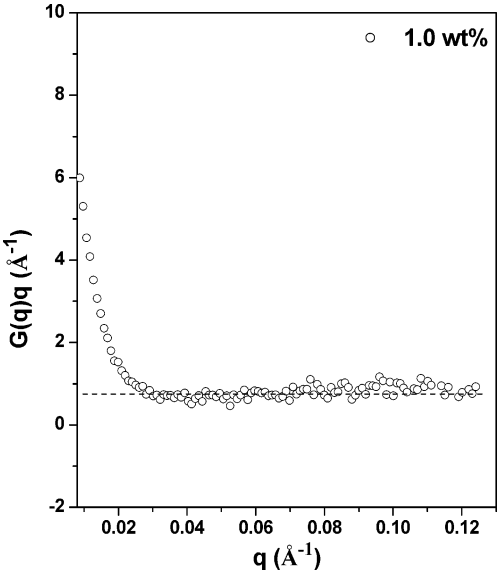

Figure 2. $g(q)q$ vs q plot of 1.0 wt % DP6−PPV/chloroform solution for the determination of the molar mass per unit length (M_L) from the asymptotic value of the plot.

$$P_{rod}(q) = \frac{I(q)M_u}{cN_{av}z\Delta\rho^2\upsilon_u{}^2} = \frac{G(q)}{z} \quad (3)$$

In the high-q limit, $P_{rod}(q) \rightarrow \pi/(qL)$[15], eq 3 thus translates to

$$\lim_{q\to\infty} G(q) = \frac{I(q)M_u}{cN_{av}\Delta\rho^2\upsilon_u{}^2} = zP_{rod}(q) = \frac{\pi M_u z}{qLM_u} = \frac{\pi M_L}{M_u q} \quad (4)$$

where M_L is the molar mass per unit length of the rod. Equation 4 prescribes that the product of $g(q)$ and q reaches an asymptotic value given by $\pi M_L/M_u$. Figure 2 displays the $g(q)q$ vs q plot for the 1.0 wt % DP6−PPV/chloroform solution. The plot was generated using the following parameter values: $\rho_{DP6-PPV} = 1.321 \times 10^{10}$ cm^{-1}, $\rho_{chloroform-d} = 3.16 \times 10^{10}$ cm^{-2}, and $\upsilon_{u,DP6-PPV} = 5.73 \times 10^{-22}$ cm^3. M_L determined from the plateau was 4.3 gmol^{-1} nm^{-1}. This value closely agreed with the molar mass per unit length of the monomer unit of DP6−PPV (=5.0 gmol^{-1} nm^{-1}) calculated by dividing the molecular weight of the monomer unit (M_u = 338 g mol^{-1}) by the length of a monomer unit (=6.7 Å).[35] This attested that the rod entity probed in the high-q region corresponded to the rodlike segments constituting DP6−PPV chains.

The conformation of semirigid polymers is usually described by the "wormlike chain" possessing relatively large persistent length, l_{ps} (l_{ps} < contour length).[36−39] In the low-q region ($q < l_{ps}{}^{-1}$) where the global conformation is probed, the wormlike chain approaches the coil behavior and the corresponding form factor exhibits an asymptotic power law of $I(q) \sim q^{-\nu}$ with ν = 2.0 and 1.7 in θ and good solvent, respectively.[40] Rodlike behavior corresponding to the rigid nature of the polymer chain on local

(35) Huang, Y. F. Ph.D. Thesis, Institute of Material Science and Engineering, National Sun Yat-Sen University, Taiwan, 2002.
(36) Aime, J. P.; Bargain. F.; Fave. J. L.; Rawiso, M. Schott, M. *J. Chem. Phys.* **1988**, *89*, 6477.
(37) Aime, J. P.; Bargain. F.; Schott, M.; Eckhardt, H.; Miller, G. G.; Elsenbaumer, R. L. *Phys. Rev. Lett.* **1989**, *62*, 55.
(38) Des Cloizeaux, J. *Macromolecules* **1973**, *6*, 403.
(39) Yoshizaki, T.; Yamakawa, H. *Macromolecules* **1980**, *13*, 1518.
(40) Rubinstein, M.; Colby, R. H. *Polymer Physics*; Oxford: New York, 2003.

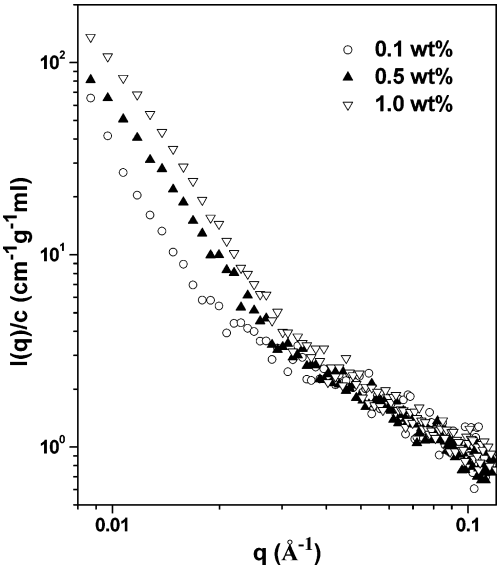

Figure 3. The concentration-normalized SANS profiles of DP6−PPV/chloroform solutions. $I(q)/c$ in the low-q region was found to increase with increasing overall polymer concentration, indicating that DP6−PPV exhibited significant interchain aggregation.

scale emerges in the high-q region ($q > l_{ps}^{-1}$). In principle, the persistent length of the wormlike chain may be determined from the crossover (q_c) from the rodlike behavior to the coil behavior via $l_{ps} = 3.5/q_c$,[37−39] provided that the scattering profile over the q range of interest represents the form factor of the single chain or the subchain that is long enough to manifest the wormlike behavior. Exact determination of l_{ps} was however implausible here because, as will be shown later, the scattering profiles at $q < \sim 0.03$ Å^{-1} in Figure 1 were not dominated by the form factor of molecularly dissolved DP6−PPV chains. Nevertheless, the fact that the q^{-1} power law extended to ca. 0.03 Å^{-1} indicated that l_{ps} of the chain was larger than 3.5/0.03 Å^{-1} =117 Å.

The scattering intensities of DP6−PPV/chloroform solutions exhibited obvious upturns at $q < \sim 0.03$ Å^{-1}, where the corresponding slope in the log−log plot became ca. −2.7 and was virtually independent of concentration. Therefore, the scattering profiles of the three concentrations shared essentially the same feature, namely, the intensities exhibited a power law of $I(q) \sim q^{-2.7}$ in the middle- to low-q region, but this q-dependence transformed to $I(q) \sim q^{-1}$ at high q corresponding to the rodlike behavior of the chain segment. Since polymer chain conformation usually depends weakly on concentration, the observed SANS profiles may be ascribed intuitively to the form factor of the molecularly dissolved polymer chains in the solution. However, the power law exponent of 2.7 at low-q was not prescribed by the asymptotic scattering behavior of wormlike chain or other form factor models of linear polymer chains. The attribution of the observed scattering pattern to single-chain form factor was further ruled out by the strong concentration dependence of the *concentration-normalized* intensity ($I(q)/c$), as shown in Figure 3. It can be seen that, instead of collapsing onto a single master curve, the concentration-normalized intensity in the low-q region increased with increasing overall polymer concentration.

The concentration dependence of $I(q)/c$ was not prescribed by the dynamic network structure formed by the interchain overlap in the semidilute solution either, because in this case $I(q)/c$ should *decrease* with increasing concentration in the low-q region ($q < \xi_d^{-1}$, with ξ_d being the dynamic mesh size), as $I(q)/c$ is proportional to the mesh size, which decreases with the increase of concentration.[40]

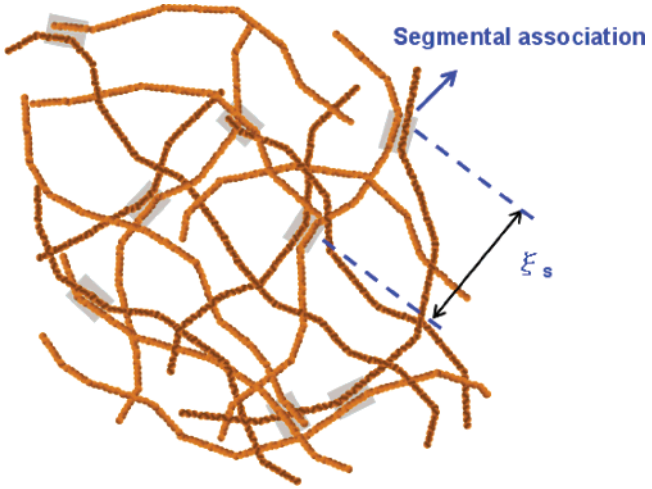

Figure 4. Schematic illustration of the network aggregates formed by DP6−PPV in the solution state. The networks were looser in chloroform but became highly compact in toluene.

The larger $I(q)/c$ at higher concentration was attributable to the significant aggregation of DP6−PPV chains in chloroform. We asserted that the observed SANS profiles were overwhelmed by the structure of the interchain aggregates. In this case, the power law of $I(q) \sim q^{-2.7}$ signaled that over the length scale covered by the low-q region the structure of the aggregates was characterized by a mass fractal dimension of ca. 2.7 irrespective of polymer concentration. The proximity of the observed fractal dimension to that (=2.5) displayed by the percolation clusters suggested that the aggregates of DP6−PPV were networks generated by the segmental association of the polymer chains, as schematically illustrated in Figure 4. The sites of the segmental association acted as the (physical) junction points for the chains (with the average distance between the junction points denoted by ξ_s). Two structural levels of the aggregates were hence probed by the SANS profiles. At $q > \xi_s^{-1}$, the scattering behavior was dominated by the form factor of the subchains between the junction points in the networks. If ξ_s was smaller than the Kuhn length of the chain, these subchains were essentially rodlike and hence gave rise to the q^{-1} power law in the high-q region in Figure 1. At $R_g^{-1} \ll q < \xi_s^{-1}$ (with R_g being the radius of gyration of the aggregates), where the structure at a more global length scale dominated the scattering behavior, the intensity displayed another power law of $I(q) \sim q^{-2.7}$ characterizing the fractal dimension of the networks. Consequently, the overall scattering profile exhibited a crossover from q^{-1} to $q^{-2.7}$ with decreasing q. Similar crossover between the power law of q^{-1} and $q^{-\alpha}$ with α lying between 2.0 and 3.0 has also been noted recently for the scattering patterns of the aggregates of carbon nanotubes in solution state.[41]

The fractal aggregates revealed here for DP6−PPV was in clear distinction with the compact plate aggregates formed by the rodlike PPE chains.[24,25] The latter was consider to possess a uniform density,[24,25] whereas the fractal aggregates of DP6−PPV had an opened structure, as a significant fraction of the unassociated segments remained mixed with the solvent molecules contained within the aggregates (cf. Figure 4).

It can be seen from Figure 1 that the crossover between the two power-law regimes (marked by the arrow) shifted to higher q with increasing polymer concentration (e.g., from 0.022 Å^{-1} at 0.1% to 0.037 Å^{-1} at 1.0%), implying a smaller ξ_s at higher polymer concentration due to higher degree of segmental

(41) Bauer, B. J.; Hobbie, E. K.; Becker, M. L. *Macromolecules* **2006**, *39*, 2637.

Table 1. Values of the Parameters Obtained from the Unified Equation Fits for DP6−PPV/Chloroform Solutions

	0.1 wt %	0.5 wt %	1.0 wt %
G_s	0.014 ± 0.008	0.026 ± 0.09	0.02 ± 0.012
B_s (10^3)	7.7 ± 0.45	5.9 ± 0.05	11.6 ± 1.3
P	2.71 ± 0.43	2.65 ± 0.05	2.62 ± 0.6
R_s (nm)	8.5 ± 2.9	6.4 ± 1.1	4.4 ± 0.9
ξ_s (=$12R_s^2)^{1/2}$ (nm)	29.4	22.1	15.2

association. We attempted to deduce the quantitative value of ξ_s through fitting the SANS profile by the "unified equation" developed by Beaucage.[42,43] The unified equation describes the scattering profiles of fractal objects in terms of hierarchical levels of structure in the system. Each structural level is described by a Guinier's law and a structurally limited power law. The unified scattering function in terms of two structural levels is given by[42,43]

$$I(q) \cong \left\{ G \exp\left(-\frac{q^2 R_g^{\,2}}{3}\right) + B \exp\left(-\frac{q^2 R_s^{\,2}}{3}\right)\left(\frac{1}{q^*}\right)^P \right\} + \left\{ G_s \exp\left(-\frac{q^2 R_s^{\,2}}{3}\right) + B_s\left(\frac{1}{q_s^*}\right)^{P_s} \right\} \quad (5)$$

where $q^* = q/[\mathrm{erf}(qkR_g/6^{1/2})]^3$ and $q_s^* = q/[\mathrm{erf}(qkR_s/6^{1/2})]^3$ with $k \approx 1.05$; $G = N_p \Delta\rho^2 V_p^{\,2}$, with N_p and V_p being the number of particles in the scattering volume and the volume of the particle, respectively. B and B_s are the prefactors specific to the types of power-law scattering characterized by the exponents P and P_s, respectively; they are given by

$$B = \left(\frac{GP}{R_g^{\,P}}\right)\Gamma\left(\frac{P}{2}\right) \quad (6)$$

$$B_s = \left(\frac{G_s P_s}{R_s^{\,P_s}}\right)\Gamma\left(\frac{P_s}{2}\right) \quad (7)$$

where Γ is the gamma function. For the present system, the first two terms in eq 5, which revealed the fractal feature of the aggregates, dominated the intensity at $q < \xi_s^{-1}$. The last two terms, which dominated the intensity at $q > \xi_s^{-1}$, captured the building block (i.e., the rodlike subchains between the junction points) with the characteristic radius of gyration of R_s of the networks.

Because the Guinier region prescribed by the R_g of the aggregates was not accessible over the q range of the present SANS experiment due to relatively large aggregate size, the first term in eq 5 was omitted for the fitting. For the curve fitting we have fixed $P_s = 1.0$ (corresponding to the power-law exponent of the rodlike subchains), thereby leaving B, G_s, B_s, R_s, and P as the fitting parameters. The fitted results were displayed by the solid curves in Figure 1, and the numerical values of the parameters obtained from the fits are listed in Table 1. The fractal dimensions, P, obtained from the fits were close to those estimated directly from the slopes of the intensity profiles in log−log plots.

R_s corresponded to the radius of gyration of the rodlike subchains between the junction points, ξ_s, and was hence given by $\xi_s \approx (12R_s^2)^{1/2}$. The values of ξ_s thus calculated were 29.4, 22.1, and 15.2 nm for the concentrations 0.1%, 0.5%, and 1.0%, respectively. The smaller ξ_s at higher polymer concentration signaled a higher degree of segmental association, as having also been manifested by the shift of the crossover between the two power-law regimes to higher q.

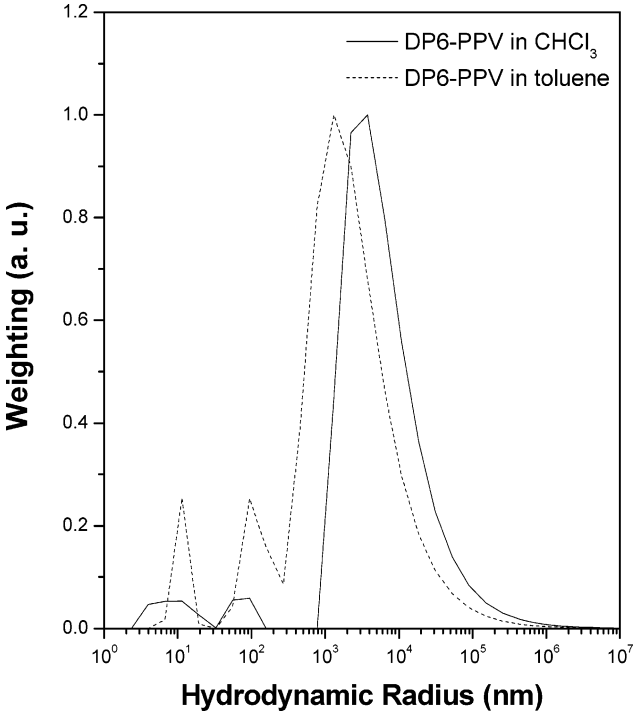

Figure 5. The distribution of hydrodynamic radius R_h in the 1.0 wt % chloroform and toluene solutions at 25 °C. The R_h profile displayed three peaks with each stemming from a characteristic relaxation mode in the system. The largest R_h was attributed to the average hydrodynamic radius of the aggregates in the solution, while the two small peaks were attributed to the internal relaxation mode of the networks and the motions of the rodlike segments.

Since the accessible q range in the present SANS experiment did not allow the R_gs of the aggregates to be determined, a DLS experiment was conducted to reveal the hydrodynamic radii, R_h, of the aggregates. Figure 5 shows the distribution of R_h in the 1.0 wt % DP6−PPV/chloroform solution at 25 °C. The R_h profile displayed three peaks with each stemming from a characteristic relaxation mode in the system. The dynamics of DP6−PPV in the solution was hence characterized by three modes, namely, the fast, medium, and slow modes. The largest R_h of 3.8 μm associated with the slow mode may be attributed to the average hydrodynamic radius of the aggregates in the solution. Consequently, the interchain aggregation of DP6−PPV in chloroform generated relatively large aggregates micrometers in size; down to the nanometer length scale the internal structure of the aggregates could be described by a rather well-defined fractal dimension of ca. 2.7. The physical range of mass fractal dimension d_m is between 1.0 and 3.0.[14,15] In general, a smaller value of d_m would imply that the structure of the fractal object is more opened or has a lower dimensionality. The rather large fractal dimension of DP6−PPV aggregates in chloroform indicated that these aggregates were quite dense in structure. It is noted that the value of the fractal dimension may also be useful for resolving the mechanism of the cluster growth from the aggregation of small subunits.[44] However, such an analysis becomes even more complex for the aggregation of long polymer chains, because the building block by itself is a fractal object.

The small peak at 72 nm (corresponding to the medium mode) in the R_h profile was attributed to the internal relaxation mode of the networks, while the other peak with $R_h \sim 8$ nm was ascribed to the motions of the rodlike segments in the aggregates. It is noted that the R_h of a rod entity is usually smaller than its

(42) Beaucage, G. *J. Appl. Crystallogr.* **1995**, *28*, 717.
(43) Beaucage, G. *J. Appl. Crystallogr.* **1996**, *29*, 134.

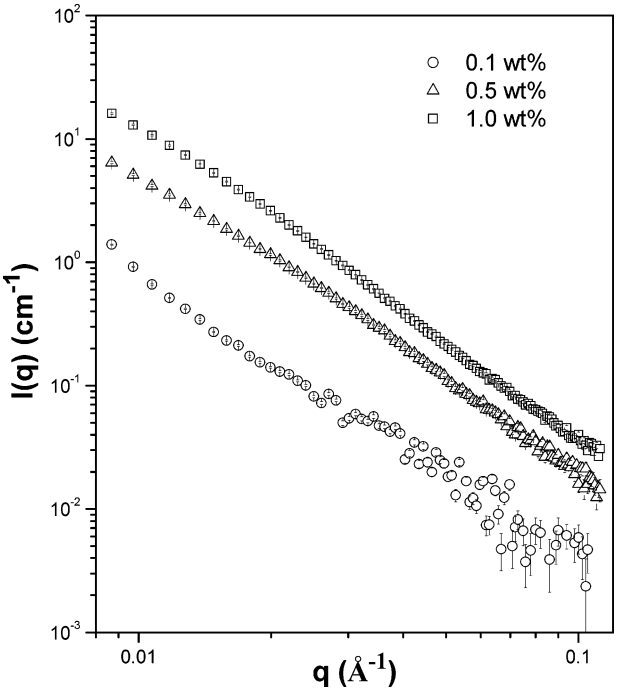

Figure 6. The room-temperature SANS profiles in log−log plots of DP6−PPV in the solutions with toluene at different concentrations. Only one asymptotic power law was identified at $q > \sim 0.02$ Å^{-1}. The corresponding power law exponents were attributed to the mass fractal dimensions of the highly compact networks formed by the interchain aggregation of DP6−PPV in the solvent.

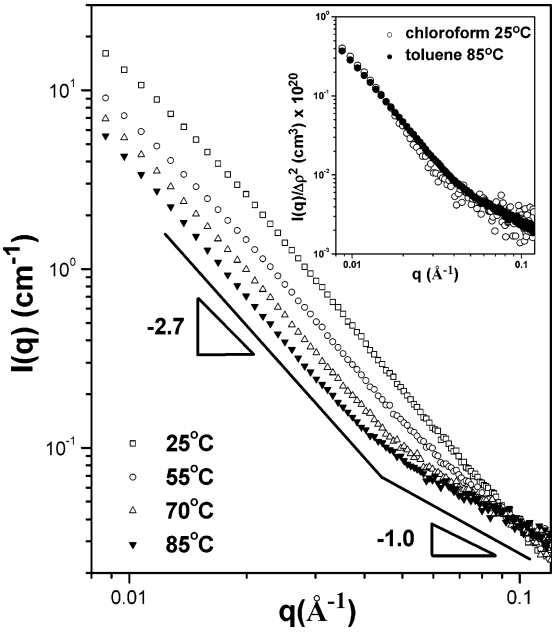

Figure 7. The temperature-dependent SANS profiles of 1.0 wt % DP6−PPV/toluene solution collected in a heating cycle. The low-q intensity depressed progressively with increasing temperature, while largely retaining its slope. Accompanied with this intensity depression was the gradual emergence of the q^{-1} power law in the high-q region. The q^{-1} regime became clear at 85 °C. The inset displays the SANS profiles normalized by the contrast factors for 1.0 wt % DP6−PPV/toluene solution at 85 °C and 1.0 wt % DP6−PPV/chloroform solution at room temperature. It can be seen that the two scattering profiles were nearly identical.

corresponding R_g.[15,45] However, as can be seen from Table 1, the radius of gyration of the rodlike subchains between the junction points ($R_s = 4.4$ nm) in the 1.0 wt % solution was smaller than the value of R_h ($\sim$ 8 nm) deduced from DLS. This discrepancy may be reconciled by considering that R_h is related not only to the size of the object but also to its dynamics of motion. In the aggregates, the motions of the rodlike subchains were indeed constrained by the junction points; therefore, the corresponding R_h became larger than that of the free rods.

Aggregate Structure in DP6−PPV/Toluene Solutions. We now turn to the structure of DP6−PPV in the poorer solvent, toluene. Figure 6 displays the room-temperature SANS profiles of DP6−PPV in the solutions with toluene. In contrast to the two distinct power-law regimes observed for the chloroform solutions, only one asymptotic power law was identified here at $q > \sim 0.02$ Å^{-1}. The corresponding slopes in the log−log plots were −2.2, −2.4, and −2.7 for the concentrations 0.1 wt %, 0.5 wt %, and 1.0 wt %, respectively. These power law exponents were again attributed to the mass fractal dimensions of the networks formed by the interchain aggregation of DP6−PPV in toluene. The absence of the q^{-1} power-law regime in the scattering profiles implied that the networks were highly compact with very small ξ_s due to severe segmental association. In this case, the q^{-1} regime was located at the region beyond the measurable q range of the SANS experiment. The smaller fractal dimensions (compared with that observed for the chloroform solutions) coupled with highly compact internal structure indicated that the aggregates in toluene tended to collapse into objects (such as disks) with lower dimensionality due to severe segmental association.

The distribution of R_h of 1.0 wt % DP6−PPV/toluene solution at 25 °C is also shown in Figure 5. The R_h profile also exhibited three peaks centering at 1.3 μm and 95 and 10 nm. The largest R_h of 1.3 μm was again attributable to the average hydrodynamic radius of the aggregates. Therefore, the aggregates in toluene were smaller than those in chloroform, due to more compact internal structure. The other two peaks corresponded to the network internal relaxation mode and the motion of the rodlike segments. The R_h associated with the former was larger than that found for the chloroform solution, as the corresponding motion became more restricted due to higher degree of segmental association in the aggregates.

Owing to the higher boiling point of toluene, a temperature-dependent SANS experiment was conducted to examine the effect of elevating temperature on the aggregation behavior of DP6−PPV in this solvent. Figure 7 displays the SANS profiles of 1.0 wt % toluene solution collected in situ at different temperatures in the heating cycle. The low-q intensity depressed progressively with increasing temperature, signaling the occurrence of de-aggregation upon heating. Interestingly, the fractal dimension of the aggregates remaining in the solution was found to remain at ca. 2.7, as the low-q slope in the log−log plot was essentially unaffected by increasing temperature. Accompanied with the depression of the low-q intensity was the gradual emergence of the q^{-1} power law in the high-q region ($q > 0.04$ Å^{-1}). The q^{-1} power-law regime became clear at 85 °C, which was about the highest achievable temperature before the intervention of solvent boiling. In this case, the scattering pattern was characterized by two distinct power-law regimes and became nearly identical with the room-temperature SANS profile of the corresponding chloroform solution after being normalized by the respective neutron contrast factors (cf. the inset in Figure 7).

The temperature-dependent SANS experiment hence revealed that heating the toluene solution tended to reduce the degree of segmental association in the network aggregates. The segmental dissociation loosened the networks, and the increase of ξ_s shifted the q^{-1} power-law regime to the accessible q range. Although the aggregates became less compact at higher temperature, their

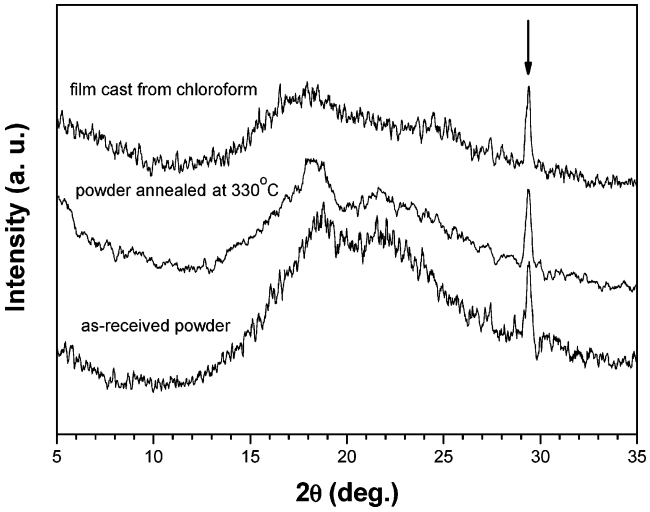

Figure 8. The WAXS scans of the as-received DP6−PPV powder used for the solution preparations, the powder having been annealed at 330 °C and the film cast from chloroform. A peak associated with $\pi-\pi$ complex was observed at 29° for all samples.

fractal dimension remained essentially unperturbed. It is further noted that the interchain aggregation was never completely dissipated even by heating to 85 °C, at which the aggregate structure was analogous to that in chloroform at room temperature. The results suggested that two types of segmental association with distinct stability existed in the aggregates of DP6−PPV. The first type was prevalent in the poorer toluene solvent and could be disrupted by moderate heating. The other type of segmental association was highly stable in the sense that they could neither be solvated by the good solvent such as choroform nor be dissipated thermally at 85 °C in toluene.

The Nature of the Segmental Associations. Here we attributed the highly stable segmental association to the $\pi-\pi$ complex already present in the DP6−PPV powder used for the solution preparation. This kind of complex was formed by the in-plane stacking of the phenylene or phenyl moiety in DP6−PPV, and the characteristic distance of ca. 3.0 Å between the aromatic groups forming the complex would lead to a peak at $2\theta \approx 29°$ in the wide-angle X-ray scattering (WAXS) profile.[46] Figure 8 shows the WAXS scan of the DP6−PPV powder used for the solution preparations. The two peaks located at 18 and 22° corresponding to the interplanar spacing of 4.9 and 4.0 Å, respectively, were associated with the packings of the aliphatic side chains of DP6−PPV.[35] A $\pi-\pi$ complex peak was clearly discernible at $2\theta = 29°$. This scattering peak was found to persist even after annealing the powder at 330 °C (cf. Figure 8), showing that the $\pi-\pi$ complex was highly stable. The WAXS profile of a DP6−PPV film cast from chloroform solution with a very rapid solvent removal is also displayed in Figure 8. It can be seen that the $\pi-\pi$ complex peak still existed, which implied that the complex present in the powder remained unsolvated in chloroform, such that it was transferred into the film after solvent removal. Consequently, the WAXS results suggested the presence of a highly stable $\pi-\pi$ complex in DP6−PPV powder. This species could neither be solvated by chloroform nor be disrupted by heating; as a result, the chains tied firmly by the $\pi-\pi$ complex formed network aggregates in the solution. This interchain clustering reduced the entropy of mixing of the polymer compared with the case where all the chains were uniformly dispersed. In the poorer toluene solvent further segmental association might then take place within the preexisting aggregates to reduce the free energy of the system. This segmental association might be driven by the amphiphicility of the DP6−PPV segments, since toluene was a relatively poor and good solvent for the aliphatic side chains and the aromatic backbone, respectively. In contrast to the $\pi-\pi$ complex, the "micelle-like" segmental association thus generated had a poorer thermal stability and could be disrupted by moderate heating.

Conclusions

On basis of the SANS and DLS study, DP6−PPV was found to exhibit interchain aggregation in solutions with both chloroform and toluene. The aggregation generated relatively large network aggregates with their internal structures characterized by the mass fractal dimensions of 2.2−2.7. In chloroform, the segmental association was attributed to the $\pi-\pi$ complex already present in the DP6−PPV powder used for the solution preparation. This highly stable complex remained unsolvated in chloroform and hence tied the polymer chains to form network aggregates. The SANS profiles associated with these networks displayed two power-law regimes characterizing the mass fractal dimension of the networks and the rodlike subchains between the junction points in the networks. Further segmental association took place in toluene due to the poor affinity of the aliphatic side chains of DP6−PPV to the solvent. The resultant aggregates were highly compact and the small ξ_s caused the shift of the q^{-1} power-law regime to the region beyond the measurable q range of the SANS experiment. The aggregates of DP6−PPV in toluene thus consisted of two types of segmental associations, namely, the $\pi-\pi$ complex, which persisted even after heating to 85 °C, and the micelle-like segmental association, which could be disrupted by moderate heating.

Acknowledgment. This work was supported by the MOE Program for Promoting Academic Excellence of Universities under the grant number 91E-FA04-2-4A. The support of NIST, U.S. Department of Commerce, and the National Science Foundation, through Agreement No. DMR-9986442, in providing the neutron research facilities used in this work, are gratefully acknowledged. Thanks are also due to Dr. Derek L. Ho at NIST for assistance in SANS experiment and helpful discussions.

LA0612769

(44) Schaefer D. W.; Martin J. E. *Phys. Rev. Lett.* **1984**, *52*, 2371.
(45) Schmidt, M. *Macromolecules* **1984**, *17*, 553.
(46) Huang, Y. F.; Yang, S. H.; Hsu, C. S.; Chen, S. A.; Su, A. C. *ICMAT International Conference on Materials for Advanced Technologies*, Singapore, 2001.